FPGA Implementation of a DTC-SVM Super-Twisting Sliding Mode Controller with Adaptive Stator Flux Observer for a Double Star Induction Motor

Fatma Zohra LATRECH*, Asma BEN RHOUMA, Adel KHEDHER

Laboratory of Advanced Technology and Intelligent Systems (LATIS), National Engineering School of Sousse (ENISo), University of Sousse, 4023 Sousse, Tunisia
adel_kheder@yahoo.fr, asma.benrhouma@yahoo.fr, fatmalatrech.2016@gmail.com (**Corresponding author*)

Abstract: This paper presents the FPGA-based implementation of the Direct Torque Control method with Space Vector Modulation (DTC-SVM) for a Double Star Induction Motor (DSIM), enhanced by a Super-Twisting Sliding Mode Controller (STSMC) and an Adaptive Sliding Mode Stator Flux Observer (SMSFO). For improving the robustness of the control system, the conventional Proportional Integral (PI) controllers are replaced by the STSMC approach. A comparative study of the Classical DTC, of the DTC-SVM-PI and DTC-SVM-STSMC methods highlights the superior performance of the proposed approach with regard to a reduced chattering, an improved electromagnetic torque control, and an increased tolerance to system parameter variations. However, despite these improvements, the proposed system remains slightly sensitive to stator resistance variations. In order to overcome this, an adaptive SMSFO based on the Lyapunov stability theory is employed for an accurate flux and torque estimation under varying stator resistance conditions. The proposed control algorithm is developed by using a VHDL code for synthesis and deployment and implemented on a FPGA board through the Xilinx System Generator (XSG). The Hardware-in-the-Loop (HIL) tests carried out confirm the enhanced dynamic performance, robustness, and real-time applicability of the proposed strategy.

Keywords: DTC, DTC-SVM-PI, DTC-SVM-STSMC, DSIM, XSG, FPGA, Adaptive SMSFO.

1. Introduction

Since their introduction in 1969, multiphase machines have attracted growing interest in the context of high-power applications due to their fault tolerance, reduced torque ripple, and modular structure (Guedida et al., 2024). Among them, the Double Star Induction Machine (DSIM), composed of two stator windings shifted by 30°, offers an excellent dynamic performance but poses complex control challenges.

Direct Torque Control (DTC) has proven to be one of the most efficient strategies for DSIM drives (Nesri et al., 2024). However, conventional DTC is affected by high torque ripple and variable switching frequency. Several methods, including fuzzy logic and sliding mode control (Latrech et al., 2023(a); Boukhalfa et al., 2022), have been proposed for improving its performance.

More recently, combining DTC with Space Vector Modulation (SVM) using Proportional Integral (PI) regulators has achieved a constant switching frequency and an improved torque response (Nahin et al., 2022). Although techniques such as fuzzy logic optimization (Reghioui et al., 2019) or multilevel inverters (Sadouni et al., 2020) further reduce torque ripple, they increase system complexity. Sliding Mode Control (SMC) has emerged as a robust alternative due to its high disturbance rejection (Ammar et al., 2020), yet its discontinuous control law causes chattering. The Super-Twisting Sliding Mode Control (STSMC) method alleviates this issue (Krim et al., 2019), but its application to DSIM remains limited and sensitive to stator resistance variation.

Accurate rotor speed is crucial for a robust control, but the encoders increase system cost and are sensitive to noise. Sensorless estimation methods have been explored for DSIM drives (Mossa et al., 2022; Sahraoui et al., 2018). In this work, an adaptive Sliding Mode Stator Flux Observer (SMSFO) is integrated into the DTC-SVM-STSMC scheme to enable a sensorless control and improve robustness against stator resistance variation (Khedher et al., 2010). For a real-time implementation, Field Programmable Gate Arrays (FPGAs) provide high-speed parallel processing in contrast to Digital Signal Processors (DSPs) or microcontrollers (El Haissouf et al., 2022). Tools such as Xilinx System Generator (XSG) simplify the development process (Latrech et al., 2023(b)). The main contribution of this paper is a robust FPGA-based DTC-SVM strategy for DSIM integrating STSMC and SMSFO in order to achieve an enhanced dynamic performance, a strong robustness, and real-time feasibility.

This paper is organized as follows. Section 2 presents the DSIM model, and Section 3 details the DTC-SVM-STSMC scheme. Section 4 describes

https://doi.org/10.24846/v34i4y202504

the adaptive SMSFO, while Section 5 discusses the simulation results. Further on, Section 6 sets forth the FPGA-based co-simulation. Finally, Section 7 concludes this paper.

2. Modelling and Extending the DTC Laws to the DSIM

2.1 DSIM Model

The voltage and flux equations of DSIM are given by equations (1) and (2):

$$\begin{cases} \bar{u}_{s1} = r_{s1}\bar{i}_{s1} + \dfrac{d\bar{\phi}_{s1}}{dt} \\ \bar{u}_{s1} = r_{s1}\bar{i}_{s2} + \dfrac{d\bar{\phi}_{s2}}{dt} \\ 0 = r_r\bar{i}_r - j\omega_r\bar{\phi}_r + \dfrac{d\bar{\phi}_r}{dt} \end{cases} \quad (1)$$

$$\begin{cases} \bar{\phi}_{s1} = L_{s1}\bar{i}_{s1} + L_{pc}\bar{i}_{s2} + m\bar{i}_r \\ \bar{\phi}_{s2} = L_{s2}\bar{i}_{s2} + L_{pc}\bar{i}_{s1} + m\bar{i}_r \\ \bar{\phi}_r = L_r\bar{i}_r + m\left(\bar{i}_{s1} + \bar{i}_{s2}\right) \end{cases} \quad (2)$$

Using the (d–q) coordinates, the DSIM model can be formulated as in equation (3):

$$\begin{cases} u_{sd1} = r_{s1}i_{sd1} + \dfrac{d\phi_{sd1}}{dt} - \omega_s\phi_{sq1} \\ u_{sq1} = r_{s1}i_{sq1} + \dfrac{d\phi_{sq1}}{dt} + \omega_s\phi_{sd1} \\ u_{sd2} = r_{s2}i_{sd2} + \dfrac{d\phi_{sd2}}{dt} - \omega_s\phi_{sq2} \\ u_{sq2} = r_{s2}i_{sq2} + \dfrac{d\phi_{sq2}}{dt} + \omega_s\phi_{sd2} \\ 0 = r_r i_{rd} + \dfrac{d\phi_{rd}}{dt} - \omega_g\phi_{rq} \\ 0 = r_r i_{rq} + \dfrac{d\phi_{rq}}{dt} + \omega_g\phi_{rd} \\ T_{em} = \dfrac{3n_p}{2}\left[\phi_{sd1}i_{sq1} + \phi_{sd2}i_{sq2} - \phi_{sq1}i_{sd1} - \phi_{sq2}i_{sd2}\right] \end{cases} \quad (3)$$

where u_s, ϕ_s and i_s denote the stator voltage, flux and current, respectively. L_{s1}, L_{s1} and L_r denote the leakage inductances of the stator windings of the first and second star, and of the rotor, respectively. Likewise, r_s and r_r are the stator and rotor resistances. L_{pc} is the mutual stator-stator inductance, while m is the cyclic mutual stator-rotor inductance. T_{em} is the electromagnetic torque, while ω_s and ω_g are the stator and slip angular speed. Likewise, ω_r is the rotor angular speed, while n_p denotes the number of pole pairs.

2.2 Extending the DTC Laws to the DSIM

The DSIM is powered by two Voltage Source Inverters (VSIs) with control signals shifted by an angle of $\pi/6$. Both voltage vectors must have the same amplitude and frequency but they are phase-shifted. In the reference frame of the first stator, the second stator's voltage appears aligned with the voltage of the first stator:

$$\bar{u}_{s1} = \bar{u}_{s2} = \bar{u}_s \quad (4)$$

Similarly, the expressions for the currents and flux are given by equations (5) and (6):

$$\bar{i}_{s1} = \bar{i}_{s2} = \bar{i}_s \quad (5)$$

$$\bar{\phi}_{s1} = \bar{\phi}_{s2} = \bar{\phi}_s \quad (6)$$

The new voltage and flux expressions in equations (7) and (8), respectively, can be written based on equations (4)-(6):

$$\begin{cases} \bar{u}_s = r_s\bar{i}_s + \dfrac{d\bar{\phi}_s}{dt} \\ 0 = r_r\bar{i}_r - j\omega_r\bar{\phi}_r + \dfrac{d\bar{\phi}_r}{dt} \end{cases} \quad (7)$$

$$\begin{cases} \bar{\phi}_s = (L_s + L_{pc})\bar{i}_s + m\bar{i}_r \\ \bar{\phi}_r = 2m\bar{i}_s + L_r i_r \end{cases} \quad (8)$$

where

$$L_{ss} = L_s + L_{pc}$$

3. DTC-SVM with STSMC for DSIM

The second-order Sliding Mode Controller enhances the first-order SMC by achieving finite-time convergence without error derivatives, thereby reducing chattering while preserving the robustness to disturbances and parameter variations (Bojan-Dragos et al., 2024). It produces smooth signals, rejects bounded disturbances, and facilitates digital implementation by avoiding higher-order derivatives.

It is simple to implement with a clear topology. The nonlinear system below is considered:

$$\dot{S} = A(x,t) + B(x,t)\cdot u_{ST}(t) \quad (9)$$

where S is the sliding surface and u_{ST} is the control signal. The unknown functions A(x,t) and B(x,t) are restricted by lower and upper boundaries.

The following conditions must be met by these functions in order to ensure that the sliding surface tends towards zero in the presence of uncertainties and disturbances:

$$\begin{cases} |A(x,t)| \le A_m \\ B_m \le B(x,t) \le B_M \\ B_m \succ 0 \end{cases} \quad (10)$$

The STSM control law is made up of two parts, u_1 and u_2, represented as follows:

$$u_{ST} = u_1(t) + u_2(t) \quad (11)$$

where:

$$\dot{u}_1 = \begin{cases} -u \text{ si } |s| \succ 1 \\ -\gamma \, \text{sign}(S) \text{ si } |s| \le 1 \end{cases} \quad (12)$$

$$u_2 = \begin{cases} -\lambda |S|^r \, \text{Sign}(S) \text{ si } |s| \prec s_0 \\ -\lambda |S|^r \, \text{Sign}(S) \text{si } |s| \le s_0 \end{cases}$$

The STSM control is tuned by a positive value of γ and by λ.

Finally, the following conditions must be satisfied to guarantee the convergence of the sliding variables:

$$\begin{cases} \lambda \succ \dfrac{A_m}{B_m} \\ \gamma^2 \ge \dfrac{4A_m}{B_m^{\,2}} \cdot \dfrac{B_m(\lambda + A_m)}{B_m(\lambda - A_m)} \\ 0 \prec r \le 0.5 \end{cases} \quad (13)$$

3.1 Synthesis of a Super-Twisting Rotor Speed Controller

The definition of the sliding surface for the STSMC speed control is as follows:

$$S_\omega = e(\omega_m) = \omega_{mref} - \omega_m \quad (14)$$

The STSMC speed control law is formulated as follows:

$$\begin{cases} T_{emref} = \lambda |S_\omega|^{1/2} \, \text{Sign}(S_\omega) + T_{emrefT} \\ \dot{T}_{emrefT} = \gamma \, \text{Sign}(S_\omega) \end{cases} \quad (15)$$

3.2 Synthesis of a Super-Twisting Stator Flux 1 and 2 Controller

The sliding surface for the STSMC stator flux 1 and 2 is defined as follows:

$$S_{\phi s1,2} = e(\phi_{s1,2}) = \phi_{sref} - \phi_{s1,2} \quad (16)$$

The STSM flux control law is given as:

$$\begin{cases} u_{sdref1,2} = \lambda |S_{\phi s1,2}|^{1/2} \, \text{Sign}(S_{\phi s1,2}) + U_{sd1,2refT} \\ \dot{u}_{sdref1,2T} = \gamma \, \text{Sign}(S_{\phi s1,2}) \end{cases} \quad (17)$$

3.3 Synthesis of a Super-Twisting Torque 1 and 2 Controller

The sliding surface for torque 1 and 2 of the STSMC is as shown below:

$$S_{Tem1,2} = e(T_{em1,2}) = T_{emref} - T_{em1,2} \quad (18)$$

The STSM torque control is as follows:

$$\begin{cases} u_{sqref1,2} = \lambda |S_{T_{em1,2}}|^{1/2} \, \text{Sign}(S_{C_{em1,2}}) + U_{sq1,2refT} \\ \dot{u}_{sqref1,2T} = \gamma \text{Sign}(S_{T_{em1,2}}) \end{cases} \quad (19)$$

Figure 1 shows the STSMC structure for torque control.

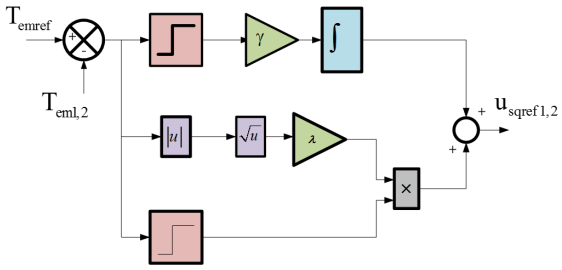

Figure 1. STSMC block diagram for torque control

4. Adaptive Sliding Mode Stator Flux Observer

In closed-loop motor drives, the encoder-based feedback may suffer from faults, noise, and mechanical issues, which reduce the overall system reliability. Sensorless estimation methods have thus been proposed, and speed was estimated through the machine model in (Khedher et al., 2010). In this work, an adaptive SMSFO is integrated for enhancing the DSIM robustness against parameter variations and disturbances, while enabling a sensorless operation and lowering the system cost. The observer is included within the DTC framework, where the voltage vector of the second stator in the selected reference frame is aligned with the voltage vector of the first stator. The proposed observer's state equation has the following form:

$$\frac{d\hat{X}}{dt} = D(\hat{\omega}_r)\hat{X} + EU + FI_S \quad (20)$$

with

$$X=\begin{bmatrix}\hat{i}_{s\alpha}\\ \hat{i}_{s\beta}\\ \hat{\varphi}_{s\alpha}\\ \hat{\varphi}_{s\beta}\end{bmatrix},\quad U=\begin{bmatrix}u_{s\alpha}\\ u_{s\beta}\end{bmatrix},\quad E=\begin{pmatrix}-\frac{L_r}{\Delta} & 0 & 0 & 0\\ 0 & -\frac{L_r}{\Delta} & 0 & 0\\ 1 & 0 & 0 & 0\\ 0 & 1 & 0 & 0\end{pmatrix},$$

$$D=\begin{pmatrix}-\frac{(R_sL_r+L_{ss}R_r)}{\Delta} & -\omega_r & \frac{R_r}{\Delta} & \frac{\omega_r L_r}{\Delta}\\ \omega_r & -\frac{(R_sL_r+L_{ss}R_r)}{\Delta} & -\frac{\omega_r L_r}{\Delta} & \frac{R_r}{\Delta}\\ R_s & 0 & 0 & 0\\ 0 & R_s & 0 & 0\end{pmatrix},$$

$$I_s=\begin{pmatrix}I_{s1}\\ I_{s2}\end{pmatrix}=\begin{pmatrix}\text{sign}(S1)\\ \text{sign}(S2)\end{pmatrix};\Delta=L_r L_{ss}-2m^2$$

The sliding surface for the SMSFO is defined based on the stator current estimation error as given by equation (21), where A^{-1} is given as follows:

$$S=\begin{pmatrix}S_1\\ S_2\end{pmatrix}=A^{-1}\begin{pmatrix}i_{s\alpha}-\hat{i}_{s\alpha}\\ i_{s\beta}-\hat{i}_{s\beta}\end{pmatrix}$$
$$\text{where } A=\begin{pmatrix}\frac{R_r}{\Delta} & \frac{\omega_r L_r}{\Delta}\\ -\frac{\omega_r L_r}{\Delta} & \frac{R_r}{\Delta}\end{pmatrix} \tag{21}$$

In cases where the digital current measurement is highly accurate, it can be assumed that there is no observation error in the respective measurement. Under such conditions, the current gain matrix can be simplified and expressed as follows:

$$\begin{pmatrix}F_{I1} & F_{i2}\\ F_{i3} & F_{i4}\end{pmatrix}=A\begin{pmatrix}\lambda_1 & 0\\ 0 & \lambda_2\end{pmatrix} \tag{22}$$

where λ_1, λ_2 are two positive constants, which are determined by applying the stability conditions, defined according to the Lyapunov approach.

To calculate the flux correction gain, convergence toward the sliding surface (S=0) is assumed. This condition allows to express the flux correction matrix as follows:

$$\begin{pmatrix}F_{\varphi 1} & F_{\varphi 2}\\ F_{\varphi 3} & F_{\varphi 4}\end{pmatrix}=\begin{pmatrix}q_1\lambda_1 & 0\\ 0 & q_2\lambda_2\end{pmatrix} \tag{23}$$

where q_1 and q_2 are positive constants. Using the Lyapunov stability theory for estimating the stator resistance error ΔRs, the Lyapunov function's derivative can be expressed by the following equation:

$$\dot{V}=\begin{pmatrix}S_1 & S_2\end{pmatrix}^T A^{-1}\frac{dE_i}{dt}=$$
$$\begin{pmatrix}S_1 & S_2\end{pmatrix}^T A^{-1}\begin{bmatrix}\begin{pmatrix}\frac{R_r}{\Delta} & \frac{\omega_r L_r}{\Delta}\\ -\frac{\omega_r L_r}{\Delta} & \frac{R_r}{\Delta}\end{pmatrix}\begin{pmatrix}E_{\varphi\alpha}\\ E_{\varphi\beta}\end{pmatrix}\\ -\begin{pmatrix}F_{i1} & F_{i2}\\ F_{i3} & F_{i4}\end{pmatrix}\begin{pmatrix}\text{sign}(S1)\\ \text{sign}(S2)\end{pmatrix}\\ -\frac{L_r}{\Delta}\Delta R_s\begin{pmatrix}\hat{i}_{s\alpha}\\ \hat{i}_{s\alpha}\end{pmatrix}\end{bmatrix} \tag{24}$$

E_i and E_φ represent the observation errors between the real and estimated current and stator flux, respectively. It can be observed that a disturbance term appears in equation (24). This part can be represented as follows:

$$\Delta\dot{V}=-\frac{L_r}{\Delta}\Delta R_s\begin{pmatrix}S_1 & S_2\end{pmatrix}^T A^{-1}\begin{pmatrix}\hat{i}_{s\alpha}\\ \hat{i}_{s\alpha}\end{pmatrix} \tag{25}$$

To overcome the influence of this component, a new Lyapunov function is introduced, which is expressed as follows:

$$V_n=\frac{1}{2}S^TS+\frac{(R_s-R_{se})}{2q_3} \tag{26}$$

where q_3 is positive constant. The derivative of the new Lyapunov function with respect to time is given by:

$$\dot{V}_n=S^TS+\frac{(R_s-R_{se})}{q_3}\frac{dRs}{dt} \tag{27}$$

Therefore, the adaptation law of R_{se} is given as follows:

$$\begin{cases}\frac{dR_s}{dt}=-q_3\frac{L_r}{\Delta}\begin{pmatrix}S_1 & S_2\end{pmatrix}^T A^{-1}\begin{pmatrix}\hat{i}_{s\alpha}\\ \hat{i}_{s\alpha}\end{pmatrix}\\ \frac{dR_s}{dt}=-q_3\frac{L_r}{\Delta}\left(E_{i\alpha}\hat{i}_{s\alpha}+E_{i\beta}\hat{i}_{s\beta}\right)\end{cases} \tag{28}$$

5. Simulation Results

5.1 Comparison of the DTC, DTC-SVM, and DTC-SVM-STSM Control Strategies

The proposed DTC-SVM-STSMC for DSIM is evaluated through simulations under a varying reference speed and load torque Tl. The first test scenario is shown in Figure 2.

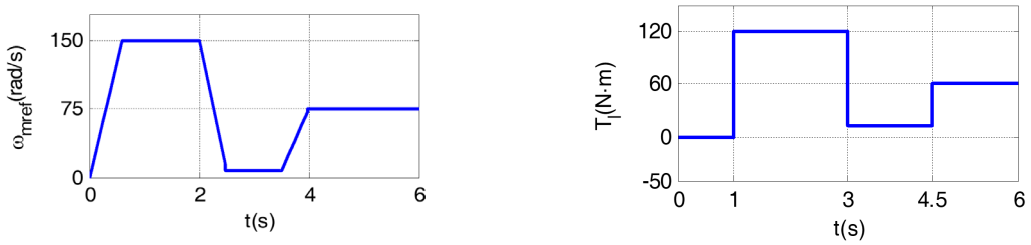

(a) (b)

Figure 2. First test scenario: (a) DSIM reference speed and (b) load torque

The DSIM parameters are provided in Appendix A.

Figure 3 illustrates the results of the first test scenario, which evaluates the performance of the DSIM under varying reference speed and load torque conditions by employing three different control strategies. As observed, all the three methods maintain a good tracking speed, confirming the robustness of DTC-based techniques in dynamic conditions.

In Figure 3(a), the motor speed behavior under load disturbances is highlighted. At t = 1 s, a load of 120 N·m causes a slight speed drop of about 2 rad/s for the conventional DTC (CDTC), 3 rad/s for DTC-SVM, and only 0.8 rad/s for DTC-SVM-STSMC. At t = 4.5 s, when a reduced load of 60 N·m is applied, the speed deviation is approximately 1 rad/s for CDTC, 1.5 rad/s for DTC-SVM, and just 0.4 rad/s for DTC-SVM-STSMC. These results clearly demonstrate that the proposed DTC-SVM-STSMC strategy exhibits a superior robustness to load changes, with a minimal impact on speed.

Figure 3(b) shows the electromagnetic torque response. All three controllers successfully track the applied torque under different speed conditions. However, the torque ripple varies significantly, reaching 0.83% for CDTC, 0.5% for DTC-SVM, and only 0.25% for DTC-SVM-STSMC. The reduced ripple obtained by the proposed method highlights its improved performance in delivering a smoother torque. A zoom-in of the torque waveform further confirms this observation.

In Figure 3(c), a magnified view of the DSIM stator current waveform under the three control strategies is shown. It is evident that DTC-SVM-STSMC achieves the lowest waveform distortion.

Figure 3(d) depicts the stator current magnitude. Again, the DTC-SVM-STSMC technique achieves the smallest ripple, indicating an enhanced current quality.

Figure 3(e) illustrates the stator flux module. The smoothness and minimal ripple achieved by DTC-SVM-STSMC confirm its advantage in flux regulation.

A quantitative comparison of ripple rates across the three employed strategies is provided in Table 1, reinforcing the superior performance of the DTC-SVM-STSMC approach for all the evaluated metrics.

The implementation of the proposed STSM control method significantly reduces the ripple levels for the stator flux and current and for the torque, as evidenced in Table 1. These outcomes underscore the enhanced effectiveness of the DTC-SVM-STSMC approach in comparison with the other two control strategies under consideration. It is well established that the Direct Torque Control performance can be sensitive to variations in machine parameters. Among these, the stator resistance Rs is particularly

Table 1. The stator flux and current and torque ripple rates for the three strategies

Ripple rates	CDTC - %	DTC-SVM - %	DTC-SVM-STSMC - %
Stator flux ripples	1.6	0.29	0.15
Torque ripples	0.83	0.5	0.25
Stator current ripples	3.68	1.5	0.75

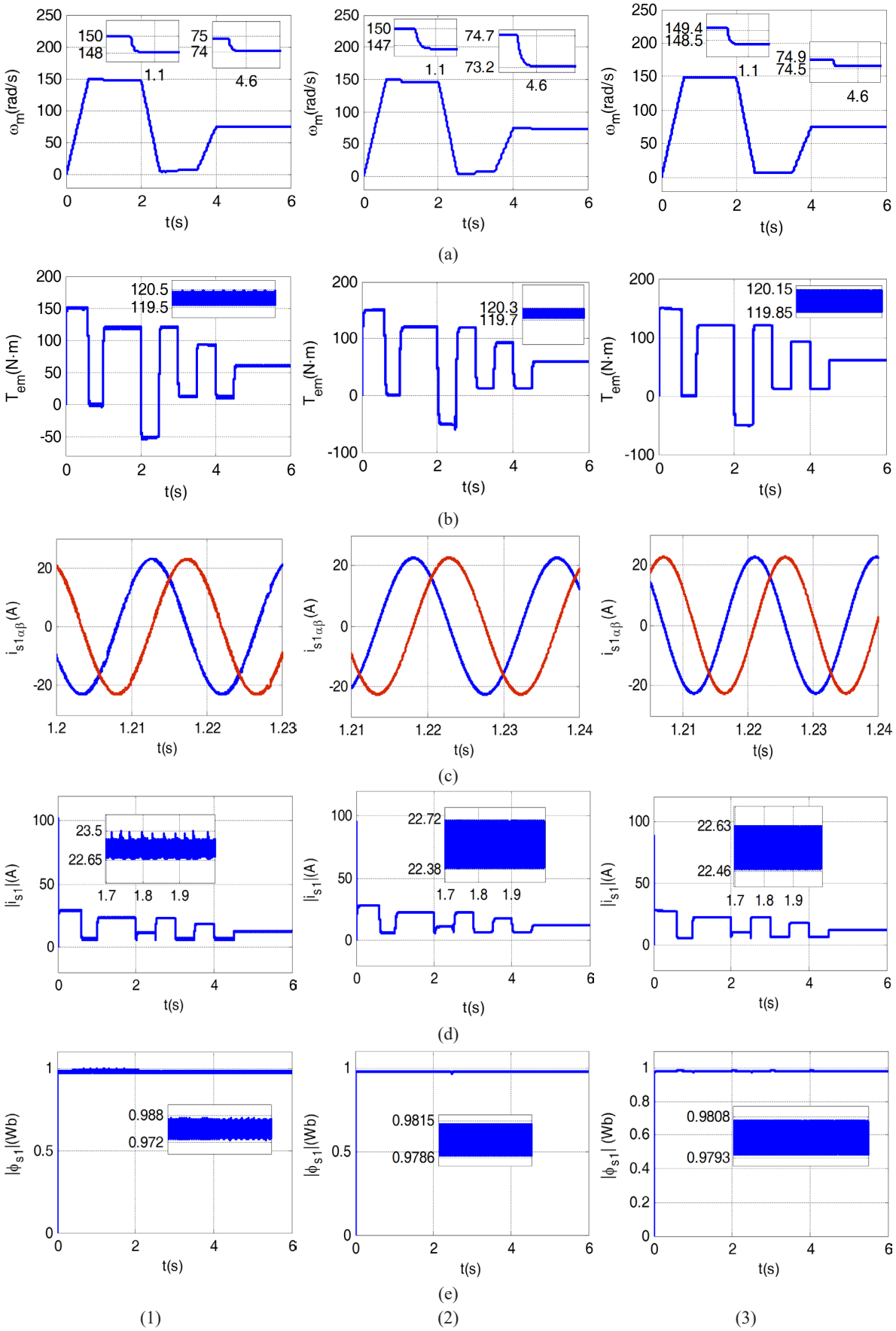

Figure 3. Simulation results for the DSIM under the three DTC strategies using the first test scenario: (a) Motor speed; (b) Electromagnetic torque; (c) Stator current waveform; (d) Stator current magnitude and (e) Stator flux module, for: (1) DTC; (2) DTC-SVM, and (3) DTC-SVM-STSMC

influential. To evaluate the robustness of the proposed DTC-SVM-STSMC method against such variations, a second simulation scenario was conducted in which Rs was reduced to 50% of its nominal value at t = 1.5 s, while the reference speed was maintained at 150 rad/s and a load torque of 120 N·m was applied at t = 1s. The comparative simulation results for the second scenario for the DSIM using the three DTC-based control strategies are presented in Figure 4. Although the stator resistance Rs variations have a low impact on motor speed, they cause notable differences in torque ripple values. Among the tested approaches, DTC-SVM-STSMC provides the lowest torque ripple and it also reduces the stator current and flux ripples, which confirms its

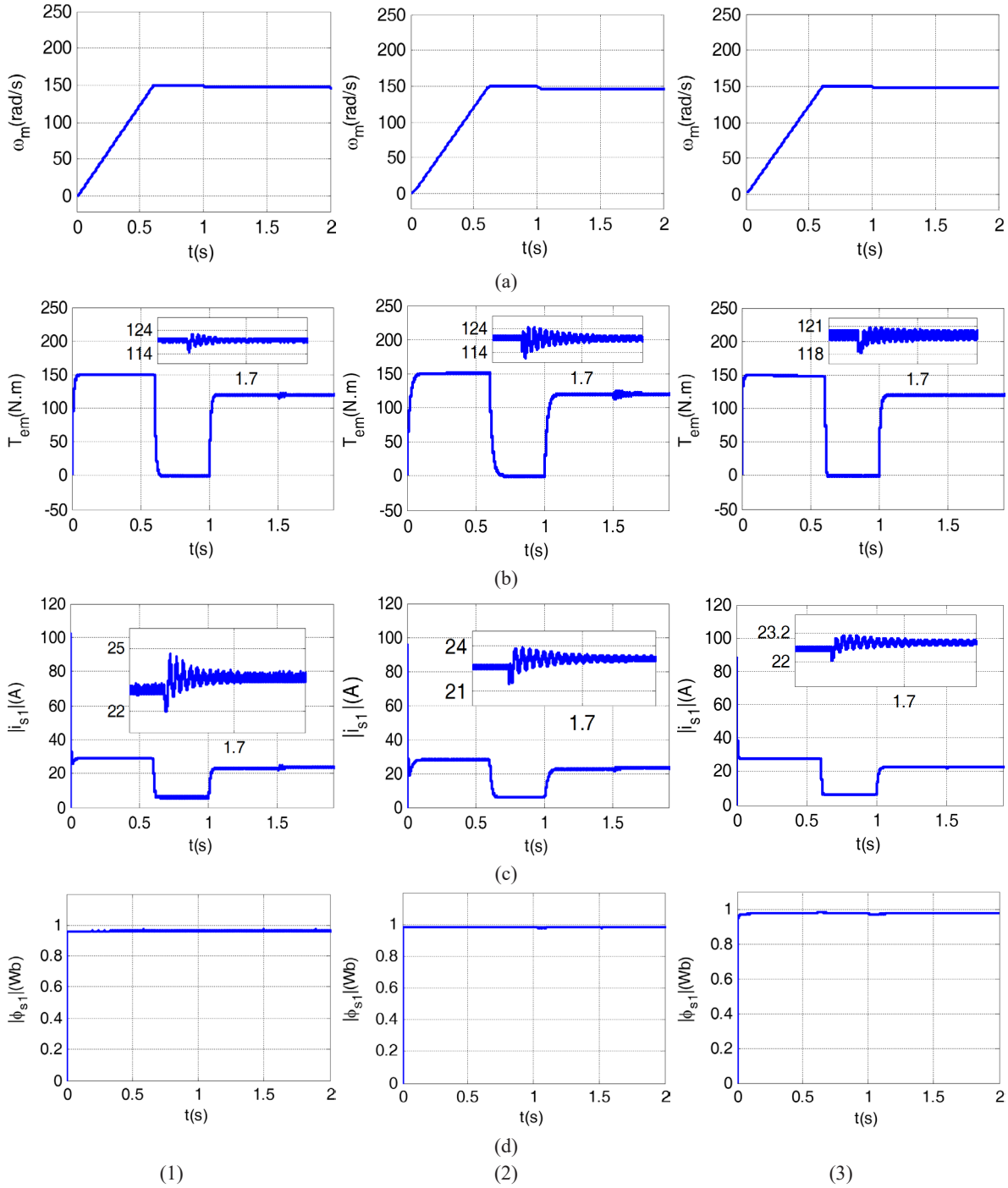

Figure 4. Simulation results for the DSIM under the three DTC strategies using the second scenario: (a) Motor speed; (b) Electromagnetic torque; (c) Stator current magnitude and (d) Stator flux module, for: (1) DTC; (2) DTC-SVM, and (3) DTC-SVM-STSMC

Table 2. The torque and stator current ripple rates with variation in Rs for the three strategies

Ripple rates	CDIC - %	DTC-SVM - %	DTC-SVM-STSMC - %
Torque ripples	8.4	8.4	2.5
Stator current ripples	12.7	12.7	5.6

higher robustness to Rs changes. Table 2 includes the torque and stator current ripple rates obtained in this scenario. However, the reduction achieved with the STSMC approach does not ensure full immunity to stator resistance variations. To enhance the adaptability of the control system to parameter variations, the conventional flux estimator is replaced by an adaptive SMSFO, which improves the flux estimation accuracy and compensates for Rs changes, thereby increasing the overall control performance.

5.2 Evaluation of the Adaptive SMSFO Performance in DTC-SVM-STSM Control of DSIM

The simulation results for the DTC–SVM–STSM control incorporating an adaptive SMSFO are depicted in Figure 5. Under the conditions of the second test scenario, the DSIM maintains a stable performance in terms of speed, torque, flux, and current despite the variations in stator resistance. This confirms the robustness provided by the embedded adaptation mechanism within the SMSFO. Additionally, the close match between the estimated and real stator resistance values validates the effectiveness of the proposed resistance estimation approach based on adaptive SMSFO. The integrated control scheme, including the adaptive SMSFO, is depicted in Figure 6.

6. Hardware in the Loop (HIL) Validation of DTC-SVM-STSMC

Hardware-in-the-Loop (HIL), alternatively referred to as hardware co-simulation, is a key approach for validating the real-time control performance on FPGA platforms. Using the Xilinx System Generator (XSG) in MATLAB/Simulink enables a direct comparison with the standard simulation results obtained in Simulink, ensuring consistency and simplifying the debugging process. For an accurate implementation, the XSG model must replicate the Simulink behavior while meeting FPGA constraints such as logic elements, memory blocks, and I/O resources (Latrech et al.,

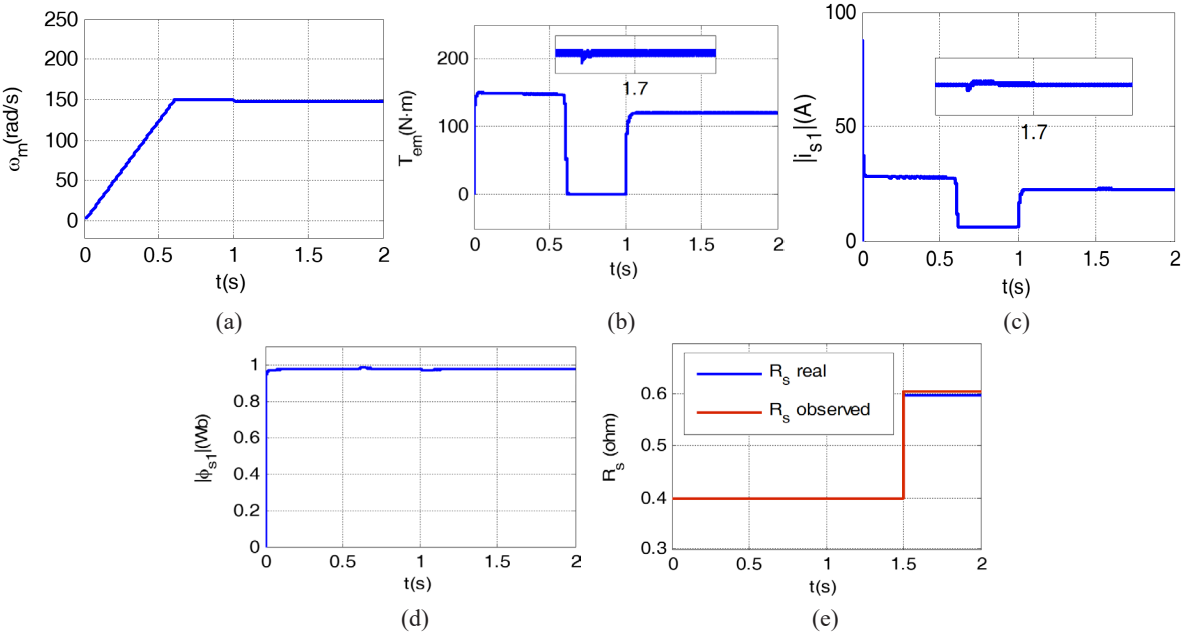

Figure 5. Simulation results for the DSIM under the DTC-SVM-STSMC method with an adaptive SMSFO control strategy: (a) Motor speed; (b) Electromagnetic torque; (c) Stator current magnitude; (d) Stator flux module and (e) observed stator resistance

2023(b)). Once these requirements are satisfied, the XSG automatically generates a VHDL code for the synthesis and deployment of DTC-SVM-STSMC, allowing the real-time validation of the proposed control algorithm on a Virtex-5 FPGA board. Figure 7 outlines the adopted hardware co-simulation methodology.

6.1 XSG-based Design of DTC-SVM-STSMC

The Xilinx System Generator (XSG), integrated with MATLAB/Simulink, is widely used for the FPGA-based control system design and validation. It offers predefined blocks for simulation and hardware testing, but some functions, such as square roots and trigonometric calculations are either absent or imprecise in the standard XSG library. To address this, custom blocks were developed in order to reproduce the Simulink functions by using the available XSG components, with a careful parameter adjustment to ensure accuracy and FPGA compatibility. An efficient data handling at block inputs and outputs, especially with counters and clock signals, is also critical. In this study, the FPGA clock period is set to 10 ns, and the DTC-SVM-STSMC strategy is implemented through interconnected blocks, including manually designed ones such as the

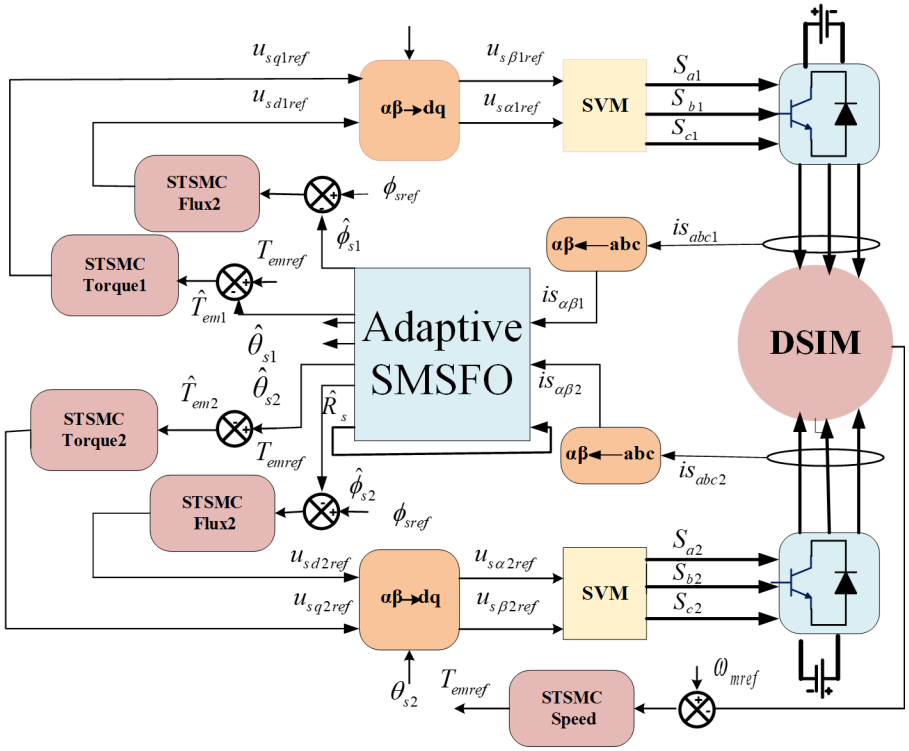

Figure 6. The block diagram of the DTC-SVM-STSMC strategy with the adaptive SMSFO

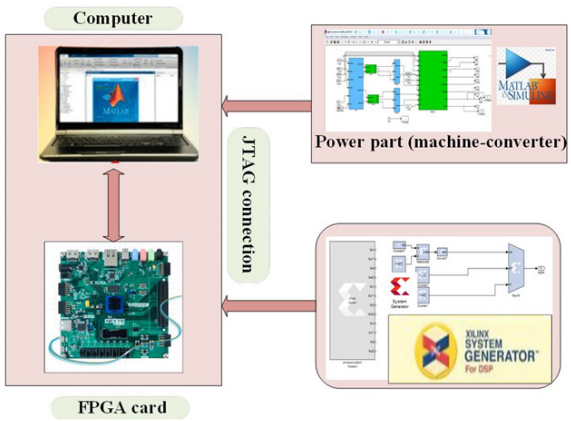

Figure 7. Block Diagram of the Co-Simulation Setup

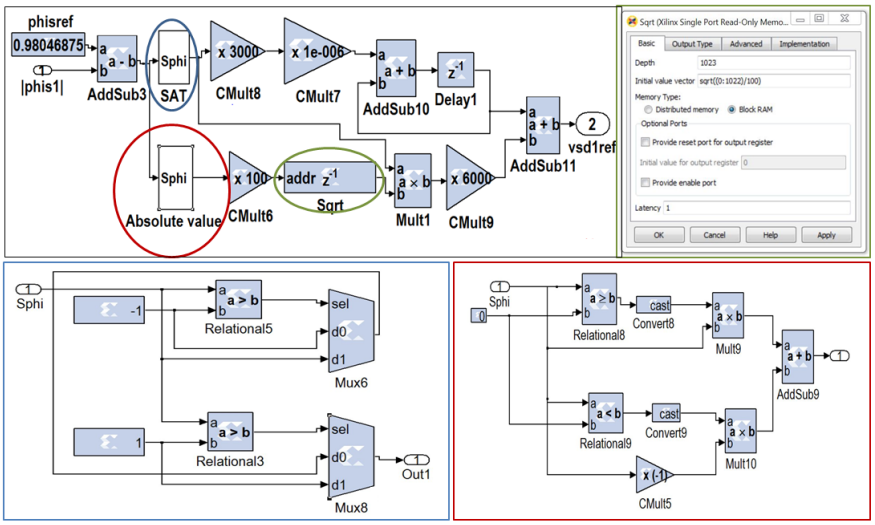

Figure 8. XSG-based Internal architecture of the Super-Twisting regulator

STSMC controller, which is not provided in the XSG library. Figure 8 shows the STSMC controller. Within this controller, a ROM block was implemented to perform the square root (sqrt) operation, which is determined by the design parameters.

6.2 XSG-based Simulation Results

Figure 9 depicts the simulation results obtained from both the XSG and Simulink environments. The errors corresponding to the difference between the values of the parameters modeled by using XSG tools and by carrying out Simulink simulations are included in Table 3. Based on these results, it can be concluded that the outputs generated using XSG closely match those obtained through numerical Simulink simulations in terms of speed regulation, stator current and electromagnetic torque response. This confirms the effectiveness and accuracy of XSG-based modeling for the design and implementation of FPGA-based control architectures.

Table 3. Errors between the XSG- and Simulink-based outcomes, in percentages

Errors	Speed	Torque	Stator current
Errors between XSG and Simulink - %	0.06	4	4.2

6.3 Hardware in the Loop (HIL) Implementation of DTC-SVM-STSMC

This subsection presents the HIL implementation of the DTC-SVM-STSMC method. After developing and simulating the control strategy, the Xilinx Integrated Synthesis Environment (ISE) is used for generating the corresponding VHDL code and performing the synthesis of DTC-SVM-STSMC. This process enables the evaluation of the proposed system`s hardware feasibility and

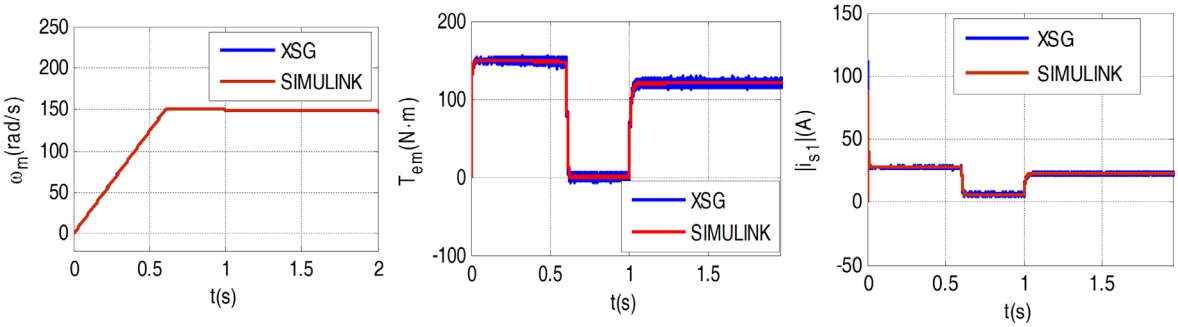

(a) (b) (c)

Figure 9. XSG and Simulink simulation results for the DSIM under the DTC-SVM-STSMC method: (a) Motor speed; (b) Electromagnetic torque and (c) Stator current magnitude

resource utilization, serving as a critical step toward a real-time FPGA implementation. The HIL implementation involves connecting the FPGA board to the PC and integrating a Joint Test Action Group (JTAG) block, generated through the Xilinx ISE environment. It is important to note that the emulation models for the DSIM motor and the inverter are incorporated within the same XSG simulation model used for the DTC-SVM-STSMC control scheme. Following the synthesis step, placement and routing are performed automatically. As a result, a programmable bitstream file, with the extension ".bit" is generated. In order to implement the real-time control strategy, this file is uploaded to the FPGA board. At this stage, the DTC-SVM-STSMC strategy is implemented by using a Register Transfer Level (RTL)-based design within the Xilinx Integrated Synthesis Environment (ISE). This RTL representation illustrates the interconnection of various functional modules, as depicted in Figure 10. The FPGA resource utilization rate for the hardware implementation of the proposed control approach is detailed in Table 4, highlighting the consumption of logic elements, memory blocks, and I/O resources and the possibility of this implementation.

7. Conclusion

This study provides a comparison between the DTC, DTC-SVM-PI and DTC-SVM-STSMC strategies employed for a DSIM. The results showed that the DTC-SVM-STSMC method achivies a superior performance by minimizing ripples for the stator flux and current and for the torque. This method also offers an improved robustness to stator resistance variations. In order to further enhance this robustness, an extension of the DTC-SVM-STSMC was proposed by incorporating an online adaptation mechanism based on an adaptive sliding mode stator flux observer. The simulation results proved that this adaptive observer effectively improves the system's robustness to stator resistance variations. Subsequently, the DTC-SVM-STSMC strategy was validated through consistent results related to both Simulink and XSG simulations, and it was successfully implemented in the framework of a hardware-in-the-loop test using a Virtex-5 FPGA.

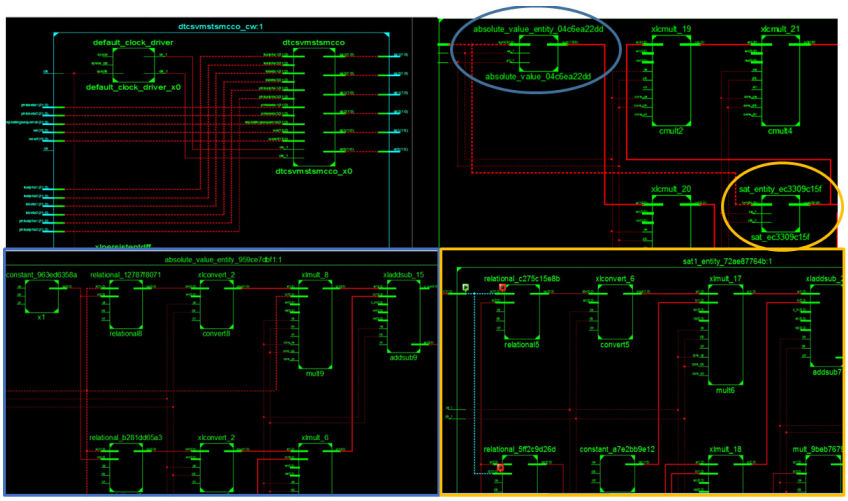

Figure 10. The RTL-based design of the DTC-SVM-STSMC method

Table 4. FPGA resource utilization summary

Logic Utilization	Used	Available	Resource utilization rate
Number of Slice Registers	2340	28800	8%
Number of Slice LUTs	4525	28800	15%
Number of fully used LUT-Fs	2001	4862	41%
Number of Bonded IOBs	205	480	42%

Appendix A. DSIM parameters

The analysed Dual Star Induction Machine operates at 220 V and 1437 rpm, with a rated torque of 120 N·m and stator currents of 2 × 19 A. Its electrical parameters include stator resistances of 0.4 Ω, a rotor resistance of 0.096 Ω, stator and rotor inductances of 82 mH and 8.9 mH, respectively, and mutual inductances of 26.3 mH (stator-rotor inductance) and 81.2 mH (stator-stator inductance). Mechanically, it features a moment of inertia of 0.6 kg·m², a viscous friction coefficient of 0.8 N·m·s/rad, and it has two pole pairs.

REFERENCES

Ammar, A., Bourek, A. & Benakcha, A. (2020) Robust SVM-direct torque control of induction motor based on sliding mode controller and sliding mode observer. *Frontiers in Energy*. 14(4), 836-849. https://doi.org/10.1007/s11708-017-0444-z.

Bojan-Dragos, C.A., Precup, R.E., Petriu, E.M. et al. (2024) Sliding Mode and Super-Twisting Sliding Mode Control Structures for Vertical Three-Tank Systems. *Studies in. Informatics and. Control*. 33(3), 5-16. https://doi.org/10.24846/v33i3y202401.

Boukhalfa, G., Belkacem, S., Chikhi, A. et al. (2022) Fuzzy-second order sliding mode control optimized by genetic algorithm applied in direct torque control of dual star induction motor. *Journal of Central South University*. 29(12), 3974-3985. https://doi.org/10.1007/s11771-022-5028-3.

El Haissouf, M., El Haroussi, M. & Ba-Razzouk, A. (2022) DSP In the Loop implementation of an Enhanced Direct Torque Control for Induction Motor Drive. In: *2022, 2nd International Conference on Innovative Research in Applied Science, Engineering and Technology (IRASET), 3-4 March 2022, Meknes, Morocco.* New York, USA, IEEE. https://doi.org/10.1109/IRASET52964.2022.9738073.

Guedida, S., Tabbache, B., Nounou, K. et al. (2024) Reduced-Order Fractionalized Controller for Disturbance Compensation Based on Direct Torque Control of DSIM with Less Harmonic. *Electrica*. 24(2), 450-462. https://doi.org/10.5152/electrica.2024.23194.

Khedher, A. & Mimouni, M. F. (2010) Sensorless-adaptive DTC of double star induction motor. *Energy Conversion and Management*. 51(12), 2878-2892. https://doi.org/10.1016/j.enconman.2010.06.028.

Krim, S., Gdaim, S. & Mimouni, M. F. (2019). Robust Direct Torque Control with Super-Twisting Sliding Mode Control for an Induction Motor Drive. *Complexity*. 2019(1), Art. ID 7274353. https://doi.org/10.1155/2019/7274353.

Latrech, F. Z., Rhouma, A. B. & Khedher, A. (2023a) Dual Star Induction Machine Driven by Direct Torque Control Using Sliding Mode Speed Controller. In: *2023 IEEE International Conference on Advanced Systems and Emergent Technologies (IC_ASET), 29 April - 1 May 2023*, *Hammamet, Tunisia.* New York, USA, IEEE. https://doi.org/10.1109/IC_ASET58101.2023.10151317.

Latrech, F. Z., Rhouma, A. B. & Khedher, A. (2023b) FPGA implementation of a robust DTC-SVM based Sliding Mode Flux Observer for a double star induction motor: Hardware in the loop validation. *Microelectronics Reliability*. 150, Art. ID 115118. https://doi.org/10.1016/j.microrel.2023.115118.

Mossa, M. A., Khouidmi, H. & Ma'arif, A. (2022) Robust Flux and Speed State Observer Design for Sensorless Control of a Double Star Induction Motor. *Journal of Robotics and Control (JRC)*. 3(4), 464-475. https://doi.org/10.18196/jrc.v3i4.15667.

Nahin, N. I., Hosain, M. K., Biswas, S. P. et al. (2022) An Improved Direct Torque Control Scheme for PWM Inverter Based Solar PV Array Fed Induction Motor Drives. In: *2022 12th International Conference on Electrical and Computer Engineering (ICECE), 21-23 December 2022, Dhaka, Bangladesh*. New York, USA, IEEE. pp. 304-307.

Nesri, M., Benkadi, H., Nounou, K. et al. (2024) Fault Tolerant Control of a Dual Star Induction Machine Drive System using Hybrid Fractional Controller. *Power Electronics and Drives*. 9(1), 161-175. https://doi.org/10.2478/pead-2024-0010.

Reghioui, H., Belhamdi, S., Abdelkarim, A. et al. (2019) Enhancement of Space Vector Modulation Based-Direct Torque Control Using Fuzzy PI Controller for Doubly Star Induction Motor. *Advances in Modeling and Analysis C*. 74(2-4), 63-70. https://doi.org/10.18280/ama_c.742-404.

Sadouni, R. (2020) Three Level DTC_SVM for Dual Star Induction Motor Fed by Tow Cascade VSI with DPCVF_SVM Rectifier. *Journal of Power Technologies*. 100(2), 171. https://papers.itc.pw.edu.pl/index.php/JPT/article/view/829.

Sahraoui, K., Ameur, A., & Kouzi, K. (2018) Performance Enhancement of Sensorless Speed Control of DSIM Using MRAS and EKF Optimized by Genetic Algorithm. In: *2018 International Conference on Applied Smart Systems (ICASS), 24-25 November 2018, Medea, Algeria*. https://doi.org/10.1109/ICASS.2018.8651996.